pubs.acs.org/Biomac

Article

Physiological Buffer Selection Alters the Mechanics of Hydrogels with Hydrazone Cross-Links

Daiyao Zhang, Neil J. Baugh, Narelli de Paiva Narciso, and Sarah C. Heilshorn*

Cite This: *Biomacromolecules* 2026, 27, 3222−3236

Read Online

ACCESS | Metrics & More | Article Recommendations | Supporting Information

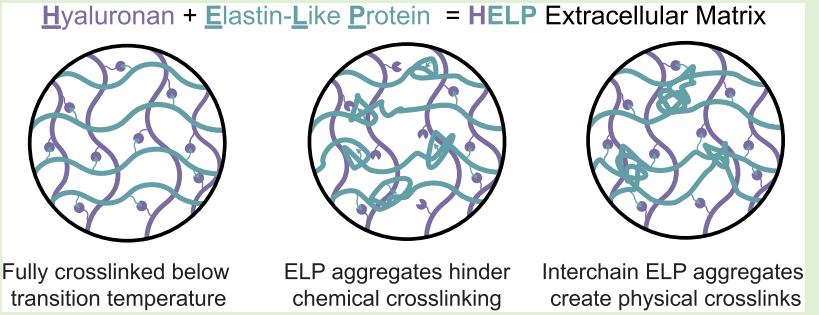

ABSTRACT: Hydrogels are used for a wide range of biomedical applications. While mechanical characterization of hydrogels is frequently performed in isotonic saline, the chemical identity of these solutions may vary widely from the ionic environments encountered during their use. To explore this idea, we test the mechanical properties of a hydrogel cross-linked with dynamic covalent chemistry (DCC) in several physiologically relevant ionic solutions that mimic different biological conditions. Specifically, we evaluate rheological properties of a hydrazone-cross-linked hydrogel composed of recombinant, chemically modified hyaluronan and elastin-like protein (ELP). Our results show that the shear moduli and stress relaxation properties of DCC hydrogels can vary significantly in different ionic environments. We identify the thermoresponsive nature of ELP and changes in hydrazone bond kinetics as the primary reasons for the observed differences in mechanical properties. Taken together, this work elucidates mechanisms underpinning changes in hydrogel mechanics in different physiological solutions.

INTRODUCTION

Hydrogels are utilized broadly throughout several applications in biomedical engineering. For example, they are used as tissue engineering scaffolds for regenerative medicine, as 3D matrices for *in vitro* cell models of development and disease,[1] as drug delivery vehicles for controlled release,[2,3] and as inks for 3D bioprinting.[4,5] Depending on the specific application, hydrogel mechanical properties must be tuned to meet the intended requirements. For instance, a common goal is to mimic the native biomechanical properties of the endogenous extracellular matrix (ECM).[1,6,7] Thus, it is critically important to accurately predict hydrogel mechanical properties during use *in operando*. Hydrogels are frequently tested for rheological properties in phosphate buffered saline (PBS) before undergoing *in vitro* or *in vivo* testing for applications.[8] However, the composition of PBS often varies from solutions experienced during actual use, which can lead to marked discrepancies between measured and actual "in-use" mechanical properties.[9,10]

In particular, prior work shows significant differences in mechanical properties for physical hydrogels when exposed to different physiologically relevant solutions.[9,11,12] Physical hydrogels are cross-linked through noncovalent interactions, such as electrostatic or hydrogen bonds, that are inherently responsive to environmental conditions including ionic concentrations and pH.[13,14] This environmental responsiveness is often exploited to design so-called "smart" hydrogels that dramatically alter their mechanical properties in different solutions. For example, ionically cross-linked hydrogels, such as alginate-based materials and many peptide-assembled systems, require a threshold of ionic strength to support gelation and to rationally tune their mechanical properties.[15,16] On the other hand, some physically cross-linked hydrogels have less intuitive responses to changes in ionic strength and character. For instance, collagen hydrogels soaked in Kokubo's simulated body fluid (SBF) were found to degrade rapidly in 14 days and lose mechanical stability, while collagen hydrogels soaked in PBS were found to erode slower and retain their mechanical characteristics.[9] Mechanical property changes like these may

Received: December 17, 2025
Revised: April 11, 2026
Accepted: April 15, 2026
Published: April 28, 2026

A

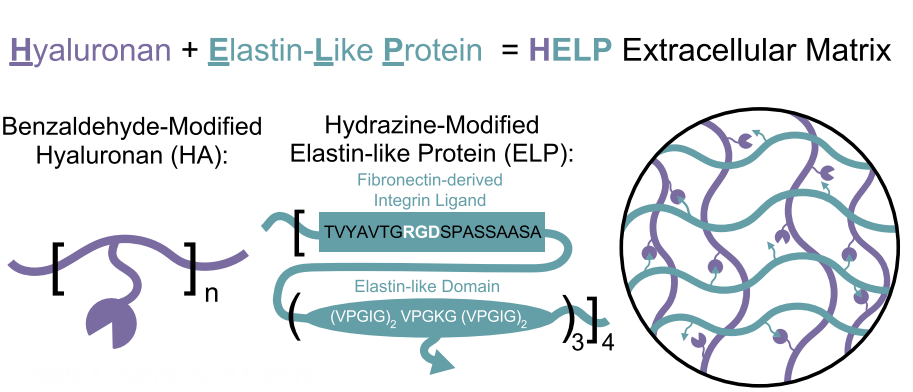

B

Biological Buffers				
	1X PBS	10X iPBS	DMEM	SBF
Phosphates (mM)	11.8	100	0.91	1
Chlorides (mM)	139.7	60	118.5	148.76
Osmolarity (mOsm/L)	313	401	326.64	356.85
Notes		Is a 10X phosphate solution	Has an organic portion	Includes sulfates, calcium

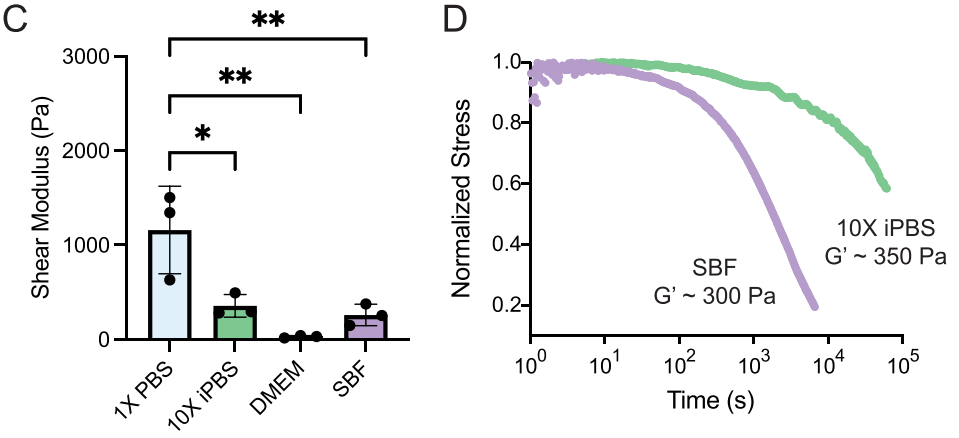

Figure 1. (A) Schematic of Hyaluronan and Elastin-Like Protein (HELP) hydrogels formulated with reversible cross-links through dynamic covalent chemistry (DCC). (B) Characteristics of biological buffers used in this study. While each of the buffers are isotonic, they differ in concentration of phosphate and chloride ions. Additional biological components are also present in DMEM and SBF. (C) Plateau shear storage moduli (G') of HELP hydrogels formulated in different biological buffers. Data are averages with SD, $n = 3$ independent gels. Statistical analysis was an ordinary one-way ANOVA with Tukey multiple comparisons correction; *$p < 0.05$, **$p < 0.01$. (D) Representative curves of normalized stress relaxation over time for HELP hydrogels formulated in SBF and 10× iPBS.

highly affect the efficacy of the hydrogel for specific biological applications.

While changes in mechanical properties of physical hydrogels in different ionic environments have been explored broadly, chemical hydrogels, *i.e.* those cross-linked with covalent bonds, have not been as widely studied in this context. Once cross-linked, ionic strength and character are not expected to modify static covalent bonds, so statically cross-linked chemical hydrogels are less responsive to different ionic solutions compared to physical hydrogels.[17] Recently, a newer type of chemical hydrogel cross-linked through dynamic covalent chemistries (DCC) has emerged within biomaterials applications.[18,19] Since the ECM is a dynamic environment, adaptable DCC hydrogels have become attractive 3D matrix mimetic platforms.[20,21]

Typically, DCC hydrogels can be made stiffer and more stable than physically cross-linked hydrogels,[22] while having adaptable self-healing properties that are lacking in covalently cross-linked hydrogels.[23] For an ideal DCC network, the hydrogel mechanical properties will be related to the thermodynamics and kinetics of the bond exchange.[24,25] For example, the hydrogel stiffness will be governed by the average

https://doi.org/10.1021/acs.biomac.5c02684
Biomacromolecules 2026, 27, 3222−3236

concentration of DCC cross-links at thermodynamic equilibrium.[26,27] In contrast, the time-dependent mechanical properties, such as the network stress relaxation rate, will be related to the bond exchange kinetics.[19,22,28−31] As the thermodynamics and kinetics of DCC reactions are known to be sensitive to solvent conditions such as pH, we hypothesized that DCC hydrogel mechanics would also be sensitive to solvent conditions, similar to the adaptable physically and ionically cross-linked gels described above.[20] For example DCC hydrogels designed with boronate ester cross-links are known to be sensitive to phosphate buffers.[32−35] Similarly, hydrazone DCC reactions are known to be sensitive to pH, with acid catalysis leading to faster exchange kinetics.[19] As hydrazone-based hydrogels are becoming more widely used for biomedical applications, we sought to explore how their mechanical behavior could be impacted by different physiological conditions.

Hydrazone-cross-linked biomaterials have been designed with both natural[36] and synthetic polymers.[37] Previously, our group formulated a DCC hydrogel made of a benzaldehyde modified hyaluronan (HA-BZA) and hydrazine modified elastin like protein (ELP-HYD).[38] Mixing these two polymers together creates a hydrogel cross-linked through hydrazone bonds, termed HELP (Figures 1A, and S1−S3).

Both HA and elastin are found within the native cell environment,[7] and the amino acid sequence of the ELP can be designed to mimic cell surface integrin binding peptides like RGD which confer cell adhesion.[39] The HELP hydrogel is both mechanically and biochemically tunable, leading to the utilization of this hydrogel in many different bioengineering applications that require specific mechanical properties.[28,40−44] Here, we employ the HELP hydrogel to explore the effects of physiological solutions on the mechanical properties of hydrazone-cross-linked hydrogels. Our results demonstrate that differences in physiological solution can significantly alter both the stiffness and the stress relaxation rate of HELP hydrogels. Because cells alter their phenotype in response to mechanosignaling induced by changes in stiffness and stress relaxation rate, these results underscore the importance of considering solvent effects when formulating DCC hydrogels for biological applications.[45−48] Using a suite of experimental methods and biologically relevant solutions (Figure 1B and Table S1), we uncover the molecular mechanisms that play a role in driving the observed differences in HELP hydrogel mechanical properties. We find that the composition and ionic strength of different physiological solutions impact polymer solubility and bond kinetics, resulting in altered mechanical properties. Taken together, this study highlights the critical importance of performing rheological characterization studies in application-relevant solutions when designing and formulating adaptable DCC hydrogels.

MATERIALS AND METHODS

Elastin-like Protein Expression and Purification

Elastin-like protein (ELP) was produced with recombinant protein expression using *Escherichia coli* BLR (DE3) cells (Novagen). pET15b plasmids containing the ELP coding sequence (Figure S1) were introduced into the BLR (DE3) cells, and the transformed bacteria were plated on Luria Broth (LB) agar (25 g/L LB; Millipore and 15 g/L agar; Millipore) supplemented with ampicillin (200 μg/mL; Thermo Fisher). Plates were incubated overnight at 37 °C. Individual colonies were then inoculated into Terrific Broth (TB, 47.6 g/L; Thermo Fisher) with 0.4% glycerol (Thermo Fisher) containing 200 μg/mL ampicillin and cultured overnight at 37 °C.

The next day, 20 mL of this starter culture was distributed into 12 one-liter baffled flasks containing fresh TB medium. Cultures were incubated at 30 °C and constantly agitated. ELP production was done using a hyperexpression strategy in which cells were grown for 24 h without induction by isopropyl β-D-1-thiogalactopyranoside (IPTG).

Purification of the expressed ELP followed previously established protocols.[38] Bacterial pellets were resuspended in TEN buffer (10 mM Tris Base, 1 mM EDTA, and 100 mM NaCl; pH 8.0). Cell lysis was achieved through three freeze−thaw cycles. Phenylmethylsulfonyl fluoride (PMSF, 1 mM; Thermo Fisher) and deoxyribonuclease I (10 μM; Sigma-Aldrich) were added to inhibit proteases and degrade nucleic acids. The lysate was subjected to three rounds of inverse transition cycling, exploiting the ELP's lower critical solution temperature (LCST) behavior and aided by the addition of salt to promote selective precipitation.

After freeze−thaw cycling, the protein solution was dialyzed at 4 °C in 10-kDa molecular weight cutoff (MWCO) tubing (Spectrum Laboratories) against 4 L of deionized water, with the deionized water replaced two to three times a day for 3 days. The dialyzed material was then passed through a 0.22-μm sterile filter, frozen, and lyophilized. The resulting dry ELP was stored at −20 °C in a sterile 50 mL tube with desiccant.

Functionalization and Characterization of ELP with Hydrazine

The ELP was functionalized with hydrazine on the primary amine of its lysine residues, following established procedures.[40,43,44,49] Briefly, lyophilized ELP was dissolved at 3% (w/v) using a 1:1 mixture of anhydrous dimethyl sulfoxide (DMSO; Sigma-Aldrich) and *N*,*N*-dimethylformamide (DMF; Sigma-Aldrich). In a separate vessel, tri-Boc hydrazinoacetic acid (used at two molar equivalents per ELP amine; Sigma-Aldrich) was dissolved in anhydrous DMF to a concentration of 2.1% (w/v) at room temperature. After dissolution, the tri-Boc reagent was activated by adding hexafluorophosphate azabenzotriazole tetramethyl uronium (HATU, 2 equiv per ELP amine; Sigma-Aldrich) and 4-methylmorpholine (5 equiv per ELP amine; Sigma-Aldrich). After 10 min, this mixture was added dropwise to the ELP solution under constant stirring, and the reaction was allowed to proceed overnight at room temperature.

To isolate the modified protein, the reaction mixture was introduced dropwise into ice-cold diethyl ether at a 1:4 ratio of ELP solution to ether, causing the product to precipitate. The precipitate was collected, dried under nitrogen overnight, and subjected to deprotection of the hydrazine moiety by resuspending the material in a 1:1 solution of dichloromethane (DCM; Sigma-Aldrich) and trifluoroacetic acid containing 5% (v/v) tri-isopropylsilane (Sigma-Aldrich). This mixture was stirred at room temperature for 4 h. The resulting deprotected ELP-HYD was again precipitated in ether, dried under nitrogen, and dissolved in deionized water before dialysis. Dialysis was carried out for 3 days at 4 °C using 10-kDa MWCO tubing (Spectrum Laboratories), with water changes two to three times daily. The final solution was filtered through a 0.22-μm membrane, lyophilized, and the resulting fibrous white solid was stored at −20 °C. Structural confirmation was performed on both the protected and deprotected ELP-HYD using ^{1}H NMR spectroscopy (Varian Inova, 600 MHz) using DMSO-d6 as a solvent (Figure S2).

Functionalization and Characterization of Hyaluronan with Benzaldehyde

Hyaluronic acid (HA) was functionalized according to established methods.[40,43,44,49] The first modification introduced an alkyne group. Sodium hyaluronate (HA, 60 kDa; LifeCore) was dissolved in MES buffer (0.2 M MES hydrate (Sigma-Aldrich) and 0.15 M NaCl in water, pH 4.5) to create a 1 wt % solution. Propargylamine (Sigma-Aldrich) was then added at 0.8 equivalence per HA dimer unit, and the reaction pH was adjusted to 6. *N*-hydroxysuccinimide (NHS; Thermo Fisher) and 1-ethyl-3-(3-(dimethylamino)propyl)-carbodiimide hydrochloride (EDC; Thermo Fisher) were both

https://doi.org/10.1021/acs.biomac.5c02684
Biomacromolecules 2026, 27, 3222−3236

introduced at 0.8 equivalence per HA dimer unit, and the mixture was allowed to react for 24 h at room temperature with continuous stirring. The product was dialyzed for 3 days against deionized water using 10-kDa MWCO tubing (Spectrum Laboratories), with two to three water changes per day, and subsequently lyophilized to yield a fibrous HA−alkyne solid.

To complete the synthesis of HA-BZA, the HA−alkyne was dissolved at 1% (w/v) in isotonic 10× iPBS (81 mM sodium phosphate dibasic, 19 mM sodium phosphate monobasic, 60 mM sodium chloride in Milli-Q water; pH 7.4; filtered through 0.22-μm membrane) supplemented with β-cyclodextrin (Sigma-Aldrich) at 1 mg/mL at room temperature. Fresh 10× stock solutions of sodium ascorbate (45.2 mM; Sigma-Aldrich) and copper sulfate (2.4 mM; Sigma-Aldrich) were prepared in MES buffer (0.2 M MES hydrate (Sigma-Aldrich) and 0.15 M NaCl in water, pH 4.5), and all solutions were degassed under nitrogen for 30 min. 4-Azidobenzaldehyde (Santa Cruz Biotechnology) was dissolved in anhydrous DMSO (Sigma-Aldrich) to be added to the reaction vessel at 1 equivalence per alkyne group. The solution was degassed for an additional 10 min, then sodium ascorbate and copper sulfate were added sequentially using an insulin syringe to reach final concentrations of 4.52 mM and 0.24 mM, respectively. Azido-BZA was added last, and the combined reaction mixture was further degassed for 10 min before stirring at room temperature for 24 h.

After the 24-h reaction period, an equal volume of 50 mM EDTA (Thermo Fisher, pH 7.0) was introduced to chelate the copper catalyst, and the mixture was stirred for an additional hour. The material was subsequently dialyzed, filtered, and lyophilized following the same procedure as above, producing a white fibrous HA-BZA product. Structural confirmation was performed using ^{1}H NMR spectroscopy (Varian Inova, 600 MHz) using D_2O as a solvent (Figure S3).

Functionalization and Characterization of Hyaluronan with Hydrazine

Synthesis of *N*-(3-azidopropyl)-2-hydrazineylacetamide was carried out prior to HA functionalization. To generate this molecule, tri-Boc−hydrazinoacetic acid (1 equivalence) was combined with azidopropyl amine (1.3 equivalence), along with EDC (1.3 equivalence) and 4-dimethylaminopyridine (0.2 equivalence), in DCM. The mixture was left to react overnight with continuous stirring. Afterward, the solvent was removed under reduced pressure using a rotary evaporator, and the crude material was purified with silica gel chromotography. The resulting Boc-protected compound was exposed to a 1:1 DCM/TFA solution for approximately 4 h to remove the protecting groups. Following deprotection, the product was precipitated into ether, yielding an oil-like yellow solid.

Subsequent HA modification followed the same procedure used for generating HA−benzaldehyde, with the exception that the newly prepared *N*-(3-azidopropyl)-2-hydrazineylacetamide replaced 4-azidobenzaldehyde as the modifying agent. Each HA dimer unit was reacted with 1 equivalence of propargylamine, EDC, NHS, and the synthesized hydrazine-containing compound. ^{1}H NMR measurements (Varian Inova, 600 MHz) were performed in D_2O to confirm product identity (Figure S4).

Physiological Buffers

Physiological buffers were created according to the recipes in Table S1. All solutions were brought to pH ∼ 7 and filtered through a 0.22-μm membrane before use.

Hydrogel Formation

All HELP hydrogels were prepared to contain a final concentration of 1 wt % ELP-HYD and 1 wt % HA-BZA in the appropriate physiological buffer. HA-BZA and ELP-HYD were each dissolved to 2 wt % in the selected solvents and allowed to equilibrate overnight at 4 °C while rotating. The pH of each 2 wt % ELP-HYD and HA-BZA solution prior to hydrogel formation was measured using Thermo Fisher pH paper strips (Figure S5). The two 2 wt % stock solutions were then combined in equal volumes on ice, to prevent ELP aggregation during mixing. Upon combining the components, hydrazone bonds formed spontaneously, yielding hydrogels with final concentrations of 1 wt % HA and 1 wt % ELP. All HA-HA hydrogels were prepared similarly, but with 1 wt % HA-HYD instead of 1 wt % ELP-HYD in the final hydrogel composition.

Rheological Measurements

A stress-controlled AR-G2 rheometer (TA Instruments) equipped with a 20 mm cone-and-plate setup was used to characterize the materials while allowing gelation to occur directly on the rheometer stage. For measurements on hydrogels soaked in different solutions, an 8 mm parallel-plate configuration was utilized. To minimize sample dehydration during all tests, heavy mineral oil was applied around the interface between the plates and the sample.

Gelation with 20 mm Cone Geometry

Standard Temperature Ramp Protocol. A time sweep was first conducted at 1% strain and 1.0 rad/s for 15 min at 23 °C to allow the material to gel under ambient conditions. The sample was then heated to 37 °C at 3 °C/min, followed by a 10 min equilibration time sweep during which the storage modulus reached a steady plateau (Figures S6A,C). To determine the gel's final stiffness, a frequency sweep (0.1−100 rad/s) was performed at 1% strain, and the storage modulus was reported at 1.0 rad/s (Figure S7).

Prolonged Temperature Ramp Protocol. A long time sweep at each temperature was conducted to ensure more complete chemical cross-linking. A time sweep was conducted at 1% strain and 1.0 rad/s for 1 h at 4 °C. The sample was then heated to 23 °C at 3 °C/min, followed by a 1 h equilibration time sweep. Finally, the sample was heated to 37 °C at 3 °C/min, followed by another 1 h equilibration time sweep (Figure S6B). Similar to above, to determine the gel's final stiffness, a frequency sweep (0.1−100 rad/s) was performed at 1% strain, and the storage modulus was reported at 1.0 rad/s.

Gelation with 8 mm Plate Geometry

To perform 24-h and 7-day hydrogel soaking experiments, HELP hydrogels were formed in 8 mm diameter molds. Gelation was performed under the same conditions as described for the standard temperature ramp protocol with the 20 mm cone geometry (15 min at 23 °C followed by 10 min at 37 °C). Hydrogels were soaked in the respective solutions for 24 h or 7 days at 37 °C before being released from the molds with a spatula as an intact disk. The disk was placed on a piece of sandpaper adhered to the rheometer stage, which was set to 37 °C. Another piece of sandpaper was adhered to the bottom of the 8 mm plate geometry surface to prevent slippage. The loading gap was adjusted until a normal force of 0.1 N was measured by the rheometer. The final storage modulus was subsequently characterized using a frequency sweep at 1% strain over 0.1−100 rad/s, with the value at 1.0 rad/s reported.

Stress Relaxation Measurements

To measure stress relaxation rates of the hydrogels, a standard gelation protocol was followed on the rheometer as described above. Following the frequency sweep, the sample remained at a 1% strain for 10 min. After this, a step stress relaxation at constant shear strain amplitude of 10% was performed, and relaxation was followed until the hydrogel relaxed to 20% of the initially measured stress, $t_{20\%}$. The data was analyzed by finding the average of at least 10 different stress data points when shear strain was initially applied to the hydrogel and normalizing the time course data set to this average.

Lower Critical Solution Temperature Measurements

ELP-HYD was prepared at 10 mg/mL in various physiological buffers. For each condition, 200 μL of the solution was transferred into a 1 mm path-length quartz cuvette. Absorbance at 300 nm was recorded using a temperature-controlled circular dichroism spectrometer (Jasco J-815). The sample was heated from 4 to 65 °C at 1 °C/min, with a 10-s equilibration period before each reading. Buffer-specific blanks were collected and subtracted from the corresponding sample measurements. Data were then normalized to the maximum optical density. The transition temperature was defined as the midpoint (0.5 normalized absorbance) of the resulting curve. All measurements were performed in triplicate.

https://doi.org/10.1021/acs.biomac.5c02684
Biomacromolecules 2026, 27, 3222−3236

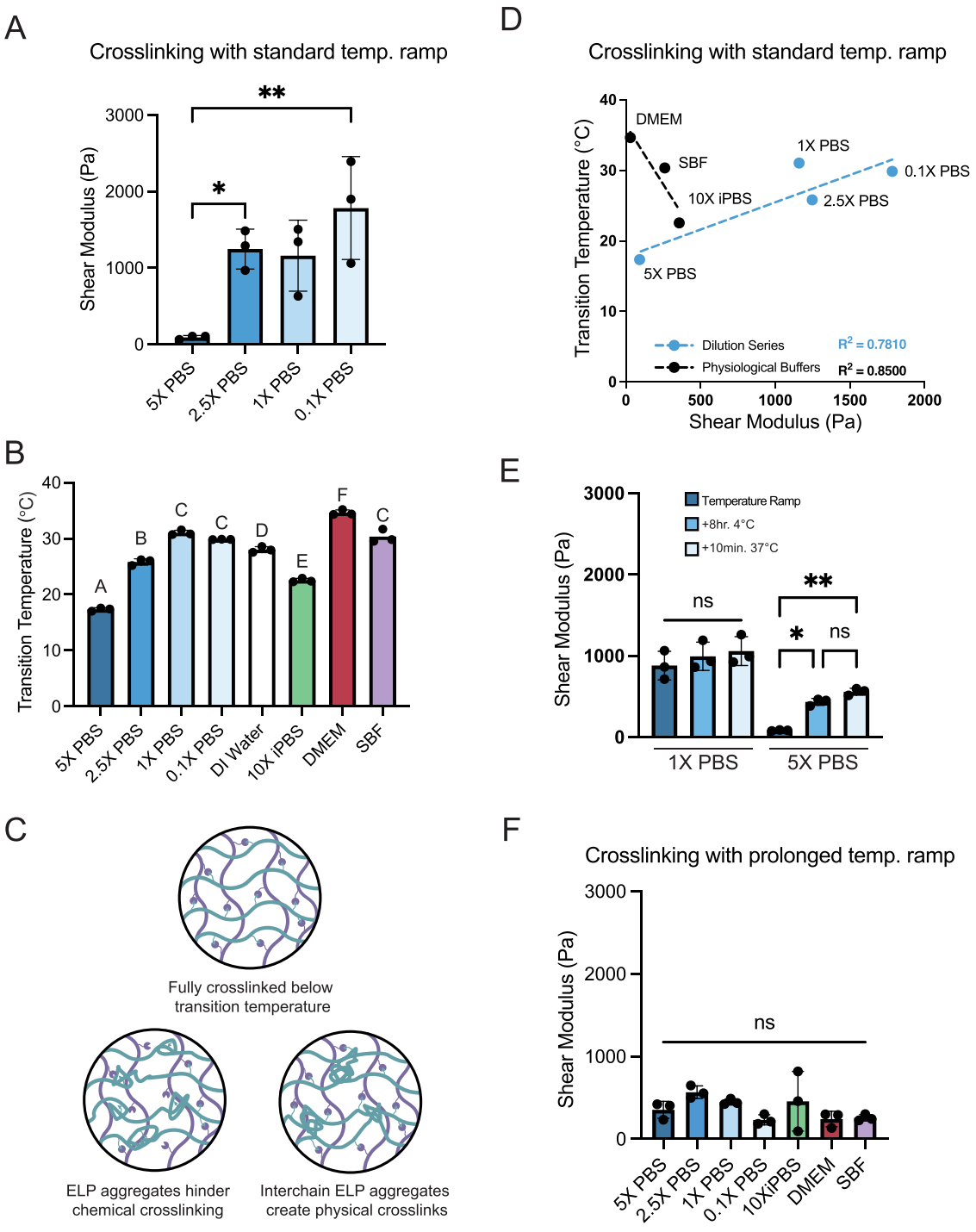

Figure 2. (A) Plateau shear storage moduli (G') of HELP hydrogels formulated in different PBS dilutions with a standard temperature ramp. (B) T_t of ELP dissolved in each buffer. Data are averages with SD, $n = 3$ independent samples. Statistical analysis was an ordinary one-way ANOVA with Tukey multiple comparisons correction; statistical significance is represented with compact letter display (CLD) where data sets that are statistically different (with $*p < 0.05$) are represented with different letters, and data sets without statistical difference share a letter. (C) Idealized schematics of HELP hydrogels with (top) full chemical cross-linking below the T_t, (bottom left) reduced chemical cross-linking due to ELP aggregate formation that obscures chemical reactive groups, and (bottom right) network with both chemical cross-links and physical cross-links due to interchain ELP aggregation. (D) Transition temperature of ELP plotted against shear modulus of HELP hydrogels after standard temperature ramp in each physiological buffer. Lines represent linear regression fits with R-squared values reported. (E) Plateau shear storage moduli (G') of HELP hydrogels formulated in different solutions after standard temperature ramp, further 8-h incubation at 4 °C, and final temperature ramp to 37 °C for 10 min. (F) Plateau shear storage moduli (G') of HELP hydrogels formulated in different solutions cross-linked with a prolonged temperature ramp protocol that includes chemical cross-linking at 4 °C for 1 h. For panels (A, E, and F): Data are averages with SD, $n = 3$ independent gels. Statistical analysis was an ordinary one-way ANOVA with Tukey multiple comparisons correction; $*p < 0.05$, $**p < 0.01$, ns = not significant.

https://doi.org/10.1021/acs.biomac.5c02684
Biomacromolecules 2026, 27, 3222−3236

Dynamic Light Scattering Measurements

Dynamic light scattering experiments were conducted using a Malvern Zetasizer Nano ZS (Malvern Instruments Ltd., UK). The set temperature was 37 °C for all measurements. HA-BZA was dissolved at 0.1 wt % and 0.22-μm filtered before 100 μL was loaded into a microcuvette (BrandTech Scientific). The measurement was repeated three times for each loaded solution, and the average was counted as one experimental replicate. Three experimental replicates were obtained for each physiological buffer condition. The hydrodynamic diameter was taken as the mean size of the majority peak as determined by volume.

Reaction Kinetics Analysis

All kinetic measurements were carried out on a UV−visible light plate reader (BioTek Synergy H1) using UV-transparent 96-well plates (Corning). For each experiment, absorbance values were corrected by subtracting a blank containing only a single model component, BZA. Both samples and blanks were prepared in triplicate (n = 3).

The characteristic absorbance wavelength for the hydrazinoacetic acid and benzaldehyde (HydAA−BZA) hydrazone bond was taken as λ_{HydAA} = 280 nm, as reported previously,[50] and the molar extinction coefficient was determined to be approximately 12000 M^{-1} cm^{-1}. For each physiological buffer, the pH of the solution was matched to be similar to that for the full-length polymers as reported in Supporting Figure S5.

For kinetic analysis, 50 μM HydAA and 50 μM BZA were mixed to a final volume of 200 μL, and absorbance readings were collected over several hours. Following blank correction, absorbance values were converted to concentration using the extinction coefficient. The resulting concentration−time profiles were then fitted in MATLAB to a reversible second-order reaction model to extract the forward and reverse rate constants. The kinetic modeling was done according to previously published work.[50]

Statistical Analysis

Across all figures, results are reported as mean ± standard deviation, with individual data points shown as black markers when applicable. Statistical comparisons were performed using a one-way ANOVA followed by Tukey's posthoc test at a significance threshold of 0.05. Significance levels are indicated as *p < 0.05, **p < 0.01, ***p < 0.001, ****p < 0.0001, and "ns" for nonsignificant differences. For data sets that include multiple overlapping significance comparisons, significance is instead conveyed using compact letter display (CLD), where groups that differ statistically (*p < 0.05) are labeled with different letters, and groups without significant differences share the same letter. All statistical analyses were conducted using GraphPad Prism 10.

Results and Discussion

Different Physiological Buffers Affect Shear Modulus and Stress Relaxation. To study the effects of different ionic solutions on HELP hydrogels, we initially selected a small panel of physiologically relevant, isotonic solvents commonly used in bioengineering research (Figure 1B, full recipes shown in Table S1). PBS is used for a wide variety of applications in cell culture and biomaterials characterization.[51,52] Other applicable ionic solutions include SBF and cell culture medium.[53] SBF mimics the inorganic composition of human blood plasma, relevant for characterizing hydrogels for *in vivo* applications.[53,54] Dulbecco's modified eagle medium (DMEM) is a popularly used cell culture medium that has also been utilized in studies observing properties of biomaterials over time.[55−58] Finally, our group has used an in-house solvent that consists of the same components and isotonic properties of PBS while containing 10× the amount of phosphates to enhance buffering capacity, which we name 10× isotonic PBS (10× iPBS).[41,43]

To evaluate the impact of solvent choice on the shear modulus of HELP hydrogels, each component was dissolved in each buffer and kept at 4 °C overnight. Both components were mixed at 4 °C on the rheometer stage before quickly bringing the temperature to 23 °C for 15 min, ramping the temperature to 37 °C, and then holding the temperature at 37 °C for 10 min. Time sweep measurements confirm that hydrogels have reached a plateau in mechanical properties before the end of this procedure (Figure S6A). After this standard temperature ramp procedure is complete, we then perform frequency sweep measurements at 37 °C and report the shear modulus within the linear region (Figure S7). Results showed that when both the HA and ELP components are dissolved in one of the four isotonic solutions prior to gelation, the plateau shear storage modulus (*i.e.* G' or stiffness) of the resulting hydrogel can vary significantly (Figure 1C). The shear modulus of HELP hydrogels formulated in 1× PBS (∼1400 Pa) was approximately 5× stiffer compared to HELP hydrogels prepared using SBF or 10× iPBS (∼300 Pa). In contrast, gels prepared in DMEM formed significantly lower stiffness gels than other conditions (∼30 Pa). In general, these shear moduli fall within the range reported for most soft tissues (300 Pa−30,000 Pa).[6]

In addition to stiffness, hydrogel stress relaxation rate is known to significantly impact cellular responses.[42,48,59−62] Unlike traditional elastic chemical hydrogels, DCC hydrogels are viscoelastic and will undergo stress relaxation — a viscoelastic property also exhibited by the native ECM.[6,7,60,63] To explore if solvent properties impact HELP gel stress relaxation behavior, we selected two solutions (SBF and 10× iPBS) that resulted in similar HELP gel stiffness (G' ∼ 300 and ∼350 Pa, respectively). Upon application of a constant stress, we observed significant differences in relaxation behavior from the two gels, despite their similar stiffness (Figure 1D). Specifically, HELP hydrogels formulated in SBF relaxed about 35× faster than hydrogels prepared in 10× iPBS (time required for HELP gels to relax 20% of their initial stress under constant strain ($t_{20\%}$) ∼320 s for SBF and ∼11,500 s for 10× iPBS). Although these rates of relaxation are slower than that reported for native tissues ($t_{20\%}$ ∼ 0.1 s−100 s), prior work has detailed that these rates still have potential to significantly alter cell mechanosignaling.[42,62]

To probe the molecular mechanisms underpinning these observed hydrogel mechanical differences, we next studied the different components of the HELP hydrogel in a more isolated manner. Specifically, we sequentially characterized potential changes in the chemically modified ELP, HA, and the hydrazone bonding between them.

Ion Content Impacts HELP Mechanics through ELP Solubility

ELPs exhibit a lower critical solution temperature (LCST) in aqueous solutions and undergo a phase change above their transition temperature (T_t) to form a polymer-rich phase and a polymer-lean phase.[64−66] This T_t is known to be heavily dependent on both ion identity and concentration,[67−69] prompting us to investigate if changes in ELP solubility might be partially responsible for the observed changes in HELP gel mechanics.

Previous work has shown that some ELP-based hydrogels stiffen when tuning the ELP to have a higher T_t.[70,71] In these cases, increasing T_t allows for a greater extent of cross-linking with ELP polymers in an extended formation, reducing any obscuring of cross-linking functional groups that occurs as the ELP aggregates with increasing temperature. In contrast, other works report the opposite trend, where lower ELP T_t increases hydrogel stiffness since the ELP-rich domains serve as additional cross-links.[49] Here, we hypothesize that the presence of both chemical cross-links and ELP physical cross-links will result in stiffer hydrogels, while the oversaturation of one may lead to a weaker hydrogel. To explore this hypothesis, we examined the relationship between ELP T_t and HELP shear modulus in different physiological buffers.

First, we prepared gels using a dilution series of PBS solutions (5× PBS, 2.5× PBS, 1× PBS, and 0.1× PBS) to keep ion identity the same while decreasing ionic strength. Both HA and ELP were dissolved in these solutions and cross-linked using the previously described protocol. In general, we observed that lower bulk ion concentration correlated with higher hydrogel shear modulus (Figure 2A), with gels formulated in 0.1× PBS exhibiting an approximately 10-fold higher shear modulus compared to those prepared in 5× PBS.

Next, to characterize the T_t of the ELP-HYD in each of our physiological solutions, we performed optical density measurements

https://doi.org/10.1021/acs.biomac.5c02684
Biomacromolecules 2026, 27, 3222−3236

as the temperature increased from 4 to 65 °C (Figure 2B). Overall, we observed that T_t increased as the PBS salt concentrations were diluted up to 1× PBS. Past this point, (*e.g.*, 0.1× PBS and deionized water (DI water)) a slight decrease in T_t was observed. These results are consistent with previously reported nonlinear changes in ELP LCST values as a function of chaotropic salt concentration.[67,72−74] Chaotropic ions decrease the structuring of water (*i.e.* "structure breakers"). At low salt concentrations, direct ionic binding of chaotropic anions to amides in the backbone of ELP causes a "salting in" effect, causing ELP to be more soluble compared to in deionized water.[67] However, in more concentrated salt solutions, the excess anions polarize water molecules surrounding ELP, increasing the thermodynamic cost of hydrating its hydrophobic regions and leading to a lower T_t.[67] In contrast, kosmotropic ions increase the structuring of liquid water (*i.e.* "structure makers"). Kosmotropic ions will typically "salt-out" proteins, even at low concentrations.[67] Thus, for PBS, which includes both chaotropic and kosmotropic ions, there is a parabolic relationship between ELP T_t and ion concentration.

When comparing the ELP T_t in the other physiological buffers, we must consider the role of both ion identity and concentration (Figure 2B,2C, and Table S1). The relative ability of anions and cations to modulate the solubility of proteins is commonly described through use of the Hofmeister series, a ranking of ions based on how they affect properties of solubilized proteins.[75,76] When comparing the 1× PBS and 10× iPBS (which have similar osmolarity (Figure 1B, and Table S2)), the largest difference is the presence of fewer Cl^- ions and more HPO_4^{2-} ions in the 10× iPBS buffer. In this case, Cl^- ions are considered more chaotropic, while HPO_4^{2-} ions are more kosmotropic, suggesting that the 10× iPBS may have more overall kosmotropic character compared to 1× PBS. Thus, as expected, ELP's T_t in 10× iPBS is lower than its T_t in 1× PBS.

The formulations of SBF and DMEM differ substantially from 1× PBS. Notably, SBF has the addition of tris(hydroxymethyl)-aminomethane hydrochloride (*i.e.* Tris−HCl) (Table S1). Tris−HCl is often considered more chaotropic and is frequently used to improve protein stability due to its strong pH buffering capacity.[77,78] The ELP T_t in SBF was statistically similar to that in 1× PBS. DMEM has the addition of many components including glucose, amino acids, and vitamins, which have variable effects on protein solubility depending on context.[79−81] We observed a significantly higher ELP T_t in DMEM compared to 1× PBS.

We next checked if a correlation existed between the ELP T_t and the observed differences in gel mechanical properties. Interestingly, the HELP hydrogel with the lowest shear modulus was fabricated in DMEM, the buffer with the highest ELP T_t (Figure 2D). We hypothesized that in this case, the hydrogel can undergo complete chemical cross-linking while the ELP is still soluble (Figure 2C, top panel). In contrast, for buffers with lower ELP T_t, the chemical cross-linking can occur at the same time as the physical ELP aggregation. Thus, the impact of ELP T_t on the gel mechanical properties will depend on the relative rates of these two processes (*i.e.* chemical cross-linking and ELP phase transition) and the resulting network structure.

When comparing across all physiological buffers, the correlation between ELP T_t and HELP shear modulus was not apparent (Figure 2D). For example, while 1× PBS and SBF have similar ELP T_t, hydrogels produced in SBF have much weaker mechanical properties. This is potentially because the identity of the ions alters the rate of the chemical cross-linking reaction and/or the rate of the ELP phase change, making it difficult to predict the impact on final network structure across this broad range of buffers. However, when considering only the PBS dilution series, a clear correlation was observed, with the presence of more ions resulting in lower ELP T_t and weaker hydrogels (Figure 2D). This is presumably due to ELP-rich domains forming earlier in the chemical cross-linking period, which can obscure the hydrazine cross-linking groups and lead to less effective cross-linking and weaker gels (Figure 2C, bottom left panel). Similar results have been reported previously for other ELP-based hydrogels with variable T_t.[70,71]

To test the idea that rapid ELP aggregation can obscure the hydrazine reactive groups leading to fewer chemical cross-links and weaker hydrogels, we modulated the temperature of the hydrogel post-cross-linking. After first measuring the shear modulus using our standard temperature ramp cross-linking protocol (15 min at 23 °C followed by 10 min at 37 °C), we performed an 8-h incubation at 4 °C to potentially break physical cross-links before finally reheating to 37 °C for 10 min. We chose to test hydrogels dissolved in 5× PBS and 1× PBS for comparison, since the chemical cross-linking at 23 °C occurs above the transition temperature for 5× PBS (17 °C) and below the transition temperature for 1× PBS (31 °C). For the samples made in 5× PBS, we found that the new modulus measurements significantly increased after cooling and then reheating. This aligns with our interpretation that the early formation of physical cross-links due to ELP aggregation can obscure the hydrazine groups, resulting in fewer chemical cross-links and a lower modulus hydrogel. On the other hand, hydrogels made in 1× PBS exhibited no significant difference in shear modulus after the extra 4 °C incubation period, as expected. Interestingly, the modulus of the 5× PBS hydrogel did not recover to the value of the 1× PBS hydrogel after this long incubation at colder temperature, suggesting that some physical cross-linking was not able to be untangled within this 8-h period (Figure 2E).

For non-PBS buffers, the morphology of the ELP aggregates in the final network structure may be different due to differing rates of chemical cross-linking and ELP aggregation. We hypothesize this could result in the formation of interchain aggregates (*i.e.* physical cross-links) across neighboring chains of ELP that stiffen the hydrogels (Figure 2C, bottom right panel). Notably, this reasoning would predict that lower ELP T_t would result in stiffer hydrogels (*i.e.* the opposite trend as observed for the PBS dilution series). Indeed, for the DMEM, SBF, and 10× iPBS buffers, this correlation between lower T_t and stiffer hydrogels was observed (Figure 2D).

To test the idea that interchain ELP aggregation leads to physical cross-linking that can stiffen the hydrogels, we performed the chemical cross-linking at 4 °C for 1 h before holding at 23 °C for 1 h and then 37 °C for 1 h (Figure S6B). In this procedure, ELP should be fully soluble in all tested solutions during the initial 1-h chemical cross-linking time at 4 °C. As expected, we observed that the HELP hydrogel shear moduli became statistically similar across all buffers (Figure 2F).

As a final demonstration of how ionic conditions can modify HELP hydrogel mechanics through modulation of ELP solubility, we prepared hydrogels in aqueous solutions containing one of two different salts (NaCl or NaH_2PO_4) at two different concentrations (181 mM or 90.5 mM). We found that the more dilute solutions of both types of ions resulted in higher transition temperatures and higher shear moduli (Figure S8). These data are consistent with our findings that bulk dilution of PBS buffer results in a higher ELP transition temperature, which tends to result in higher hydrogel shear modulus. When comparing the two solutions made at 90.5 mM, the hydrogel made in NaCl showed both lower transition temperature and lower shear modulus compared to the hydrogel made in NaH_2PO_4. At the higher concentration of 181 mM, the hydrogels made in NaCl and NaH_2PO_4 had similar mechanical shear moduli. Previous literature shows that increasing the concentration of individual ions can eventually result in "salting out" of ELP at lower temperatures.[67]

Thus, taken together, these data demonstrate that changes in the ELP T_t in different physiological buffers can significantly impact the resulting storage modulus of the cross-linked HELP hydrogel. As the aggregates can both hinder chemical cross-linking and form interchain aggregates that add physical cross-links to the network, the final gel mechanical properties depend on the specific ionic identity and concentration within the buffer.

Hyaluronan Has a Similar Hydrodynamic Diameter in Different Physiological Buffers

After establishing ELP T_t as one probable cause of differences in shear modulus of HELP hydrogels in different buffers, we next sought to

https://doi.org/10.1021/acs.biomac.5c02684
Biomacromolecules 2026, 27, 3222−3236

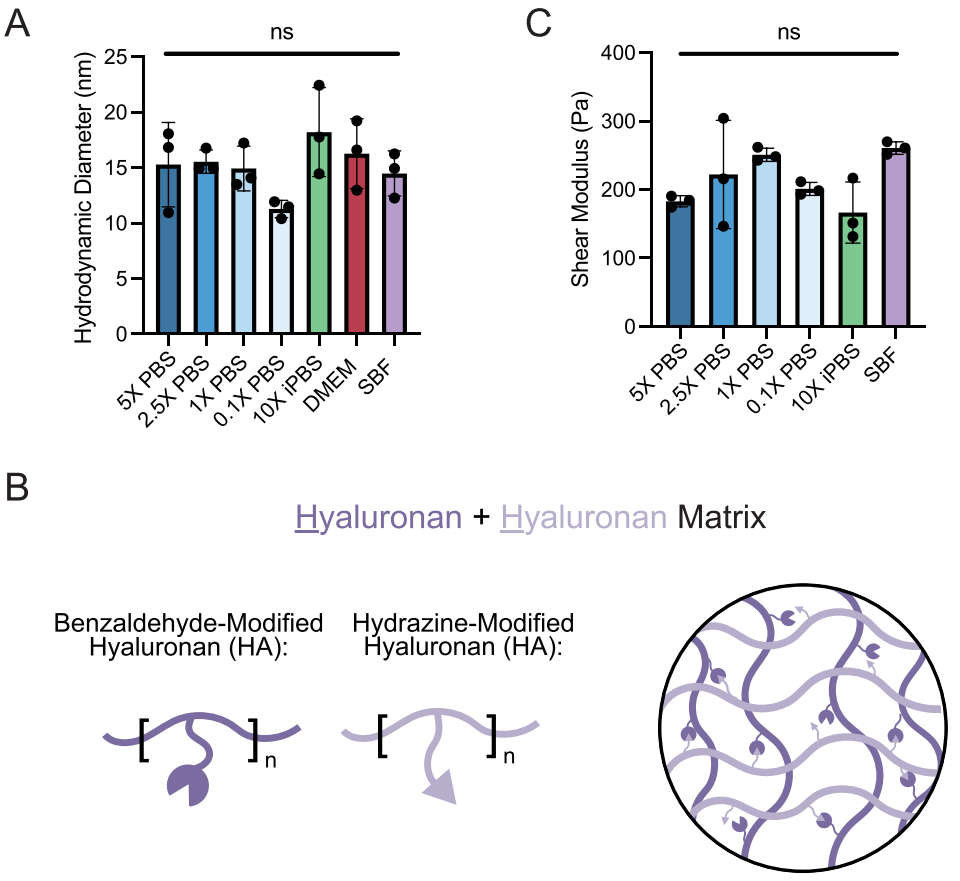

Figure 3. (A) Hydrodynamic diameter of HA-BZA dissolved in each buffer, detected using DLS at 37 °C. Data are averages with SD, $n = 3$ independent solutions. (B) Schematic of Hyaluronan-Hyaluronan (HA-HA) hydrogels formulated with reversible, hydrazone cross-links by mixing benzaldehyde- and hydrazine-modified HA. (C) Shear moduli of HA-HA hydrogels dissolved in each buffer. Data are averages with SD, $n = 3$ independent gels. For panels (A and C), statistical analyses were ordinary one-way ANOVA with Tukey multiple comparisons correction; ns = not significant.

identify if any changes in the HA component of the hydrogel also contribute to mechanical property differences.

Specifically, we wanted to explore if solution composition changed HA polymer extension at 37 °C (*i.e.* hydrodynamic diameter), as this may affect the extent of cross-linking or the force required to further extend the polymer, both of which could impact the modulus of the resulting HELP network..[82−85] While HA polymers do not exhibit an LCST, they are anionic polyelectrolytes that may have altered chain flexibility and extensibility depending on buffer ion identity and concentration.[86,87] To explore this idea, we dissolved the benzaldehyde-modified HA (HA-BZA) in the different physiological buffers and utilized dynamic light scattering (DLS) to measure average hydrodynamic diameter at 37 °C as a metric of configurational flexibility. No statistically significant differences in HA-BZA diameter were observed (Figure 3A), suggesting that HA-BZA may have similar conformational entropy across all of the physiological buffers.

These data further suggest that HA-BZA does not significantly contribute to the observed changes in HELP hydrogel mechanics in different physiological buffers. To systematically confirm this, we replaced the ELP component of the hydrogel with a hydrazine-modified HA (Figures 3B, and S4). HA-HA hydrogels were formed following identical cross-linking conditions as previously described for HELP hydrogels, with final concentrations of 1 wt % for each polymer component. Using the same standard temperature ramp as that for the HELP hydrogels, we observed that the cross-linked materials reached a plateau in mechanical moduli before the end of this procedure (Figure S6C). Oscillatory rheology for HA-HA hydrogels formed in each of the physiological buffers displayed no significant differences in shear modulus (Figure 3C). Taken together, the HA hydrodynamic diameter measurements and the HA-HA gel rheology suggest that the HA component of HELP hydrogels does not contribute significantly to differences in shear moduli in different buffer conditions. Furthermore, these data suggest that gels made only of HA biopolymers may be more resistant to stiffness changes in different ionic conditions.

Hydrazone Bond Kinetics Are Altered in Different Buffer Conditions

After characterizing the effects of ionic conditions on each of the two biopolymer components independently, we next explored the effects of ionic conditions on the chemical cross-links between the two biopolymers. Previously, we identified that the kinetic competition between physical and chemical cross-linking of HELP hydrogels directly affects the HELP shear modulus. To further explore this idea, we utilized a simplified model system to quantify hydrazone bond kinetics within different buffers in the absence of any physical cross-links. Specifically, we utilized freely solubilized benzaldehyde (BZA) and hydrazinoacetic acid (HydAA) molecules (each at 50 μM) to allow for UV spectroscopic characterization of the hydrazone concentration over time.[50,52,88] The forward and reverse reaction rate constants, k_1 and k_{-1}, respectively, along with the thermodynamic equilibrium constant (K_{eq}) were calculated by fitting the concentration over time to a second-order reaction rate (Figure 4A).[50]

Interestingly, we found that the thermodynamic equilibrium constant of the hydrazone cross-linking reaction was not significantly different between buffer conditions (Figure 4B). For a chemical hydrogel at equilibrium in the absence of physical cross-links, the shear modulus should be directly related to the number of effective

https://doi.org/10.1021/acs.biomac.5c02684
Biomacromolecules 2026, 27, 3222−3236

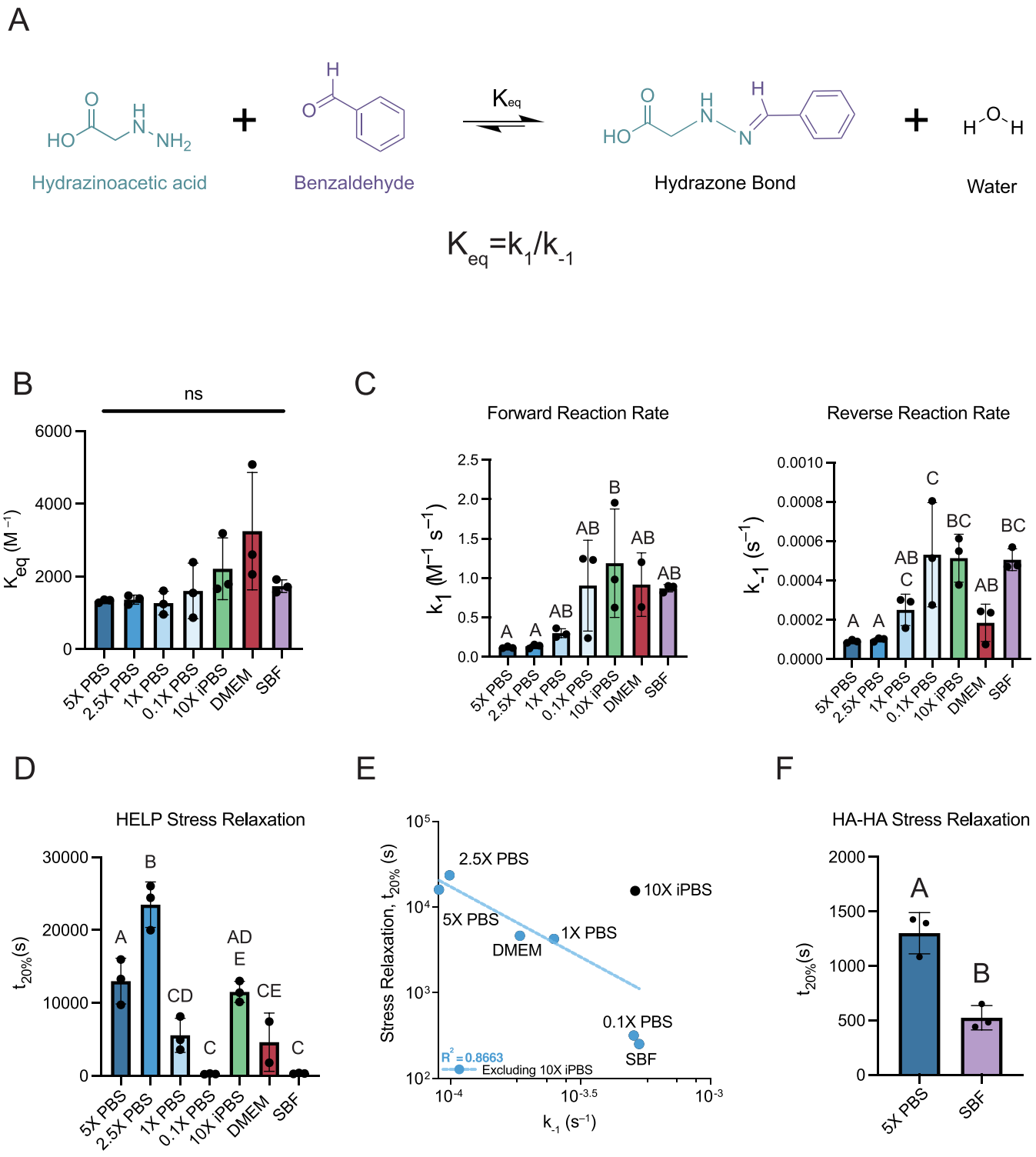

Figure 4. (A) Model reactants used to characterize hydrazone bond reaction rate constants in different buffers. (B) Thermodynamic equilibrium constant and (C) forward and reverse reaction rate constants of hydrazone bond reaction in different buffers. (D) Time required for HELP gels to relax 20% of their initial stress under constant strain ($t_{20\%}$). (E) Reverse reaction rate constants plotted against $t_{20\%}$. The dashed line with a slope of −1.6 represents fit of data excluding 10× iPBS with R-squared value reported. (F) Time required for HA-HA gels to relax 20% of their initial stress under constant strain when formulated in 5× PBS and SBF. Panels (B, C, D, F): Data are averages with SD, $n = 3$ separate hydrogels. Statistical analyses were ordinary one-way ANOVA with Tukey multiple comparisons correction; "ns" for not significant differences. Statistical significance is represented with compact letter display (CLD) where data sets that are statistically different (with at least $^*p < 0.05$) are represented with different letters, and data sets without statistical significance are represented with the same letter.

chemical cross-links at any given instant in time, which is governed by K_{eq} for a well-mixed system.[26,27,52] Consistent with this idea, HELP hydrogels chemically cross-linked at 4 °C to prevent physical cross-linking all displayed similar shear moduli across all buffers tested (Figure 2F). This further supports the idea that the observed differences in stiffness for the HELP hydrogel system when cross-

https://doi.org/10.1021/acs.biomac.5c02684
Biomacromolecules 2026, 27, 3222−3236

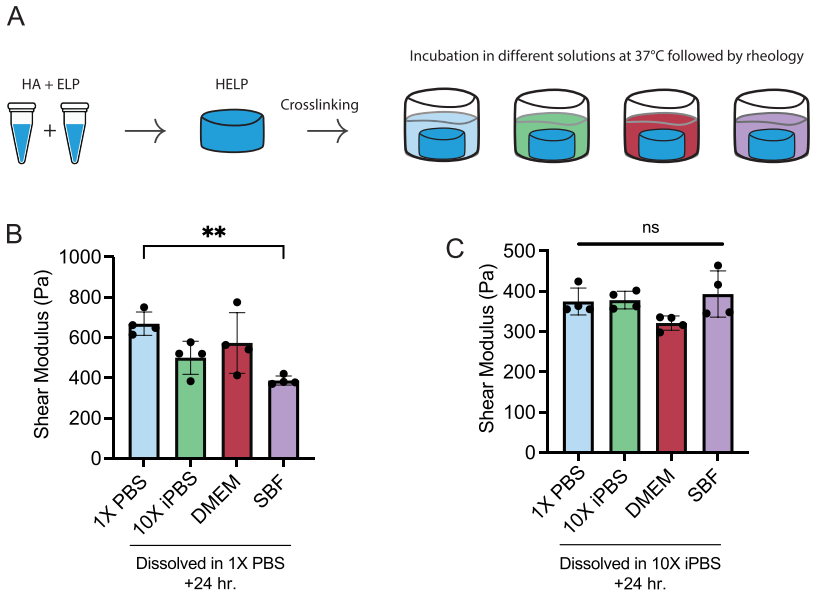

Figure 5. (A) Schematic of experimental design. Chemically modified HA and ELP are dissolved in 1× PBS or 10× iPBS, then mixed to form HELP hydrogels. Fully cross-linked hydrogels are then soaked in different physiological buffers at 37 °C before shear storage modulus measurements are performed. (B) Plateau shear storage moduli (G') of HELP hydrogels formulated in 1× PBS or (C) 10× iPBS and then soaked for 24 h in different physiological buffers. Data are averages with SD, $n = 3$ independent gels. Statistical analysis was an ordinary one-way ANOVA with Tukey multiple comparisons correction; $^{**}p < 0.01$, ns = not significant.

linked at higher temperatures are due to the competition between the kinetics of the physical and chemical cross-linking processes.

While the thermodynamic equilibrium constants were similar, the separate forward and reverse reaction rate constants were significantly different across the various ionic solutions (Figure 4C). For example, the k_1 in 10× iPBS was about eight-times higher than that for 2.5× PBS. As the effect on k_{-1} for the two buffers was approximately similar, the combined effect on K_{eq} was negligible. Thus, the observed differences in HELP shear modulus for these two formulations (Figure 2C) are likely due to changes in ELP T_t and not due to changes in hydrazone bond thermodynamics.

Given that the forward and reverse reactions rate constants had similar changes across the different buffers, this suggests that hydrazone bond catalysis is likely occurring in the different ionic solutions. General acid catalysis is known to influence the kinetics of hydrazone chemistry.[89−91] Consistent with this idea, within the PBS dilution series, lower buffering capacity (*i.e.* more dilute solutions) tended to result in more acidic hydrogel environments (Figure S5) and higher reaction rate constants (Figure 4C). Similarly, DMEM contains many amino acids that may promote hydrazone exchange through nucleophilic catalysis.[52,92,93]

For dynamic hydrogels, the kinetics of bond exchange are thought to directly influence the network stress relaxation modes.[94,95] For example, the addition of a catalyst can significantly increase the stress relaxation rate of hydrazone-cross-linked hydrogels.[28,96] Thus, we next explored if the hydrazone bond off-rates correlated with the observed hydrogel relaxation time scales. We measured the time required for the HELP gels to dissipate 20% of the initial stress upon application of a constant 10% strain ($t_{20\%}$) in each of the buffers (Figure 4D). Interestingly, the stress relaxation rate displayed significant variability for the different HELP gels. For example, gels formulated in 5× PBS had a $t_{20\%}$ that was over 100-times slower than that for gels formulated in SBF (Figure 4D), despite having similar stiffness (Figure 2D). The stress relaxation of dynamic hydrogels is closely related to the breaking of cross-links, dissipating the net stress experienced by the hydrogel.[97−99] For example, prior literature for supramolecular, guest−host hydrogels has suggested that an inverse power-law scaling exists between cross-linker kinetic off-rate and the network stress relaxation rate.[100] We observed that our HELP gel formulations followed this general power-law trend with a slope of −1.6, with the exception of hydrogels formulated in 10× iPBS (Figure 4E). This may be due to confounding effects of the ELP T_t, which we reasoned would also play a significant role in modulating the gel stress relaxation rate. Prior literature has observed that hydrogel networks with dense cross-links may create a more constrained network topology, resulting in slower stress relaxing hydrogels even in the presence of high molecular dissociation constants.[101] ELP aggregation during cross-linking would likely lead to chain entanglements that could slow down stress dissipation. Consistent with this idea, we observed a trend across all HELP gel formulations where gels with lower ELP T_t (*i.e.* more ELP aggregates) had longer stress relaxation times (Figure S9).

To separate the effects of ELP T_t and hydrazone bond kinetics on gel stress relaxation rate, we replaced the ELP-hydrazine with HA-hydrazine to formulate an HA-only hydrogel. We characterized the stress relaxation times of HA-HA gels formulated in 5× PBS and SBF, the two buffer conditions that had the largest difference in k_{-1} (100-fold). While the 5× and SBF HA-HA gels had similar shear storage moduli (182 and 260 Pa, respectively, Figure 3C), the 5× PBS gel stress relaxation time was approximately 2.5-times slower than that of SBF (Figure 4F). This confirms that the ionic conditions can have a significant impact on the exchange rate of dynamic covalent cross-links within hydrogels, and thus significantly alter their stress dissipation behavior. As the stress relaxation rate of biomaterials can have profound impacts on cell phenotype,[42,48,59−62] these results highlight the importance of considering the ionic environment when designing hydrogels to achieve specific viscoelastic properties.

Shear Modulus Is Stabilized When Initially Dissolved in Highly Buffered Solutions

After confirming that HELP hydrogel mechanics were sensitive to different buffer conditions, we next sought to identify methods to mitigate these effects. We hypothesized that initially forming the hydrogel in a solution with higher buffering capacity may allow for more stable hydrogel mechanical properties even when exposed to different ionic conditions after formation. To test this idea, we dissolved the individual ELP and HA components in either 1× PBS or the more highly buffered 10× iPBS. The solubilized HA and ELP components were mixed and incubated according to the cross-linking procedure described above (23 °C for 15 min and then 37 °C for 10 min). Following cross-linking, the hydrogels were then soaked in one of four physiological buffers for 24 h at 37 °C (Figure 5A).

https://doi.org/10.1021/acs.biomac.5c02684
Biomacromolecules 2026, 27, 3222−3236

Rheological characterization at the end of the 24-h incubation period was performed to determine the plateau shear modulus at the linear region of the frequency sweep at 37 °C. Hydrogels originally formulated in 1× PBS exhibited statistically significant differences in shear modulus when soaked in PBS and SBF, decreasing from 600 to 350 Pa, respectively (Figure 5B). In contrast, we found that HELP hydrogels originally formulated in 10× iPBS displayed statistically similar shear moduli after being soaked in each of the different buffers (Figure 5C). This suggests that hydrogels formed in 10× iPBS are more mechanically stable in response to different ionic conditions compared to hydrogels formed in 1× PBS, potentially due to the increased buffering capacity of 10× iPBS (Table S3). Thus, when preparing HELP hydrogels for *in vitro* or *in vivo* applications that are expected to encounter different ionic environments, formulating the gel in 10× iPBS may prevent unwanted changes in mechanical properties. For longer incubation periods (∼1 week), hydrogels formed in 10× iPBS maintained their mechanical properties when incubated in 1× PBS or 10× iPBS at 37 °C (Figure S10). Interestingly, when soaked in DMEM, both hydrogels formulated with 1× PBS and 10× iPBS experienced significant weakening over 7 days, potentially due to amino acid-driven hydrolysis of the hydrazone cross-links.[52] In contrast, hydrogels formulated with 10× iPBS and then incubated for 1 week in SBF experienced significant stiffening, which may be due to formation of calcium phosphate mineral deposits from the high concentration of phosphate ions in 10× iPBS in combination with the calcium ions in SBF.[102−104] Taken together, these data strongly support the measurement of biomaterial properties over time durations and in buffer conditions that mimic the intended application.

CONCLUSION

In summary, we report that a dynamic covalently cross-linked hydrogel, HELP, exhibits differences in both shear modulus and stress relaxation rate when formulated in different ionic solutions.

We found that differences in HELP hydrogel shear moduli are largely due to changes in ELP LCST transition. There exists a complex relationship between transition temperature and hydrogel shear modulus. The presence of both physical and chemical cross-links in the HELP hydrogel gives rise to a parabolic relationship between T_t and HELP hydrogel shear modulus. Very high T_t results in lower stiffness due to the absence of physical cross-links, while very low T_t also results in lower stiffness due to interference with the formation of chemical cross-links. Due to these offsetting effects, the final stiffness can be difficult to predict and will depend on processing variables such as the cross-linking temperature. Thus, for hydrogels composed of biopolymers with thermoresponsive solubility, we recommend characterizing their mechanical properties using ionic buffers that replicate the *in operando* environment as closely as possible.

Additionally, we identified that the dynamics of hydrazone bond kinetics can vary significantly in different physiological buffers, resulting in alterations in hydrogel stress relaxation behavior. Importantly, this trend was present both in hydrogels with and without ELP, suggesting that this observation is generalizable across different hydrogel formulations. Here only two gel compositions were explored: HELP and HA-HA, both with dynamic covalent hydrazone cross-links. As other biopolymeric hydrogels with hydrazone cross-links have been reported,[105−107] an interesting future direction would be to verify these trends for a more diverse range of hydrogel formulations.

Interestingly, since the forward- and reverse-reaction rates of the hydrazone bond were similarly impacted, the overall thermodynamic equilibrium constant was relatively unchanged across different buffer conditions. Thus, for HA-only hydrogels (without the thermoresponsive ELP), changing the ionic buffer had negligible impact on the gel stiffness, even though the stress relaxation rate was significantly altered. Future investigations could explore the role of ionic conditions on other types of DCC reactions with differing kinetics. Many types of DCC hydrogels[24,108] are being developed for a range of biomedical applications, and future studies should fully consider the effects of physiological solutions on mechanical properties for these new materials.[18] For example, phosphate buffers have been reported to have similar effects on the mechanical properties of boronate ester hydrogels.[32−35] Additionally, we specifically characterized the plateau shear storage modulus and stress relaxation rate, as these parameters are frequently reported in the biomaterials literature. However, depending on the application, other mechanical properties can also be critical. For example, in the field of 3D bioprinting, yield stress, extensional viscosity, and shear thinning behavior are important material properties.[109−111] Future studies could examine how changes in ionic conditions potentially alter these other important rheological properties.

Finally, our data also demonstrate that hydrogels can alter their mechanical properties when they are exposed to new ionic buffers. Interestingly, the hydrogel sensitivity was decreased when the materials were initially formulated in a solution with higher buffer capacity. Thus, our results highlight the importance of considering the full set of processing conditions and characterizing the final hydrogel mechanical properties in an environment that mimics *in operando* use. This is particularly important for hydrogels in contact with living systems, because mechanical properties are known to greatly impact cell phenotype.[42,48,59−62] Taken together, these data identify the ionic environment as a previously underappreciated factor in controlling DCC hydrogel mechanical properties.

ASSOCIATED CONTENT

Supporting Information

The Supporting Information is available free of charge at https://pubs.acs.org/doi/10.1021/acs.biomac.5c02684.

Additional experimental details include the full ELP amino acid sequence, ^{1}H NMR spectra of modified polymers, pH measurements of polymer solutions, representative hydrogel gelation graphs, shear moduli of hydrogels in other conditions, physiological buffer recipe tables, osmolarity calculations, and buffering index calculations (PDF)

AUTHOR INFORMATION

Corresponding Author

Sarah C. Heilshorn − *Department of Materials Science and Engineering, Stanford University, Stanford, California 94305, United States;* orcid.org/0000-0002-9801-6304; Email: heilshorn@stanford.edu

Authors

Daiyao Zhang − *Department of Chemical Engineering, Stanford University, Stanford, California 94305, United States*

Neil J. Baugh − *Department of Materials Science and Engineering, Stanford University, Stanford, California 94305, United States*

https://doi.org/10.1021/acs.biomac.5c02684
Biomacromolecules 2026, 27, 3222−3236

Narelli de Paiva Narciso − *Department of Materials Science and Engineering, Stanford University, Stanford, California 94305, United States*

Complete contact information is available at: https://pubs.acs.org/10.1021/acs.biomac.5c02684

Notes

The authors declare the following competing financial interest(s): S.C.H. is an inventor on a patent application (no. US2021057925) submitted by the Board of Trustees of Stanford University. All other authors declare that they have no competing interests.

■ ACKNOWLEDGMENTS

The authors thank Dr. Aidan E. Gilchrist for help on deriving reaction kinetics values through MATLAB. The authors thank Dr. Renato S. Navarro and Dr. Jordan T. Moore for fruitful discussions. The authors acknowledge funding from the National Science Foundation (NSF) DGE-1656518 (D.Z., N.J.B.), DMR 2427971 (S.C.H.), and CBET 2033302 (S.C.H.); the Stanford Graduate Fellowships (D.Z.); the National Institutes of Health (NIH) F31-HL175888 (N.J.B.), R01 EY035697 (S.C.H), R01 HL173056 (S.C.H), and R01 MH137333 (S.C.H); the ARCS Foundation Scholarship (N.J.B.); the PhRMA Foundation Predoctoral Fellowship in Drug Delivery (N.J.B.); the American Heart Association (AHA) Predoctoral Fellowship (24PRE1191604) (N.d.P.N.); and the Gerald J. Lieberman Fellowship (N.d.P.N). Part of this work was performed at the Stanford Nano Shared Facilities (SNSF), supported by the National Science Foundation under award ECCS-2026822.

■ REFERENCES

(1) Liaw, C. Y.; Ji, S.; Guvendiren, M. Engineering 3D Hydrogels for Personalized In Vitro Human Tissue Models. *Adv. Healthcare Mater.* **2018**, *7* (4), No. 1701165.

(2) Zielińska, A.; Eder, P.; Rannier, L.; Cardoso, J. C.; Severino, P.; Silva, A. M.; Souto, E. B. Hydrogels for Modified-release Drug Delivery Systems. *Curr. Pharm. Des.* **2022**, *28* (8), 609−618.

(3) Trucillo, P. Biomaterials for Drug Delivery and Human Applications. *Materials* **2024**, *17* (2), No. 456.

(4) Fang, W.; Yang, M.; Wang, L.; Li, W.; Liu, M.; Jin, Y.; Wang, Y.; Yang, R.; Wang, Y.; Zhang, K.; Fu, Q. Hydrogels for 3D bioprinting in tissue engineering and regenerative medicine: Current progress and challenges. *Int. J. Bioprint* **2023**, *9* (5), No. 759.

(5) Cao, H.; Duan, L.; Zhang, Y.; Cao, J.; Zhang, K. Current hydrogel advances in physicochemical and biological response-driven biomedical application diversity. *Signal Transduction Targeted Ther.* **2021**, *6* (1), No. 426.

(6) Chaudhuri, O.; Cooper-White, J.; Janmey, P. A.; Mooney, D. J.; Shenoy, V. B. Effects of extracellular matrix viscoelasticity on cellular behaviour. *Nature* **2020**, *584* (7822), 535−546.

(7) Saraswathibhatla, A.; Indana, D.; Chaudhuri, O. Cell-extracellular matrix mechanotransduction in 3D. *Nat. Rev. Mol. Cell Biol.* **2023**, *24* (7), 495−516.

(8) Zuidema, J. M.; Rivet, C. J.; Gilbert, R. J.; Morrison, F. A. A protocol for rheological characterization of hydrogels for tissue engineering strategies. *J. Biomed. Mater. Res. Part B: Appl. Biomater.* **2014**, *102* (5), 1063−1073.

(9) Suchý, T.; Bartos, M.; Sedlacek, R.; Supova, M.; Zaloudkova, M.; Martynkova, G. S.; Foltan, R. Various Simulated Body Fluids Lead to Significant Differences in Collagen Tissue Engineering Scaffolds. *Materials* **2021**, *14* (16), No. 4388.

(10) Tas, A. C. The use of physiological solutions or media in calcium phosphate synthesis and processing. *Acta Biomater.* **2014**, *10* (5), 1771−1792.

(11) Li, X.; Luo, F.; Sun, T. L.; Cui, K.; Watanabe, R.; Nakajima, T.; Gong, J. P. Effect of Salt on Dynamic Mechanical Behaviors of Polyampholyte Hydrogels. *Macromolecules* **2023**, *56* (2), 535−544.

(12) Rosińska, K.; Bartniak, M.; Wierzbicka, A.; Sobczyk-Guzenda, A.; Bociaga, D. Solvent types used for the preparation of hydrogels determine their mechanical properties and influence cell viability through gelatine and calcium ions release. *J. Biomed. Mater. Res. Part B: Appl. Biomater.* **2023**, *111* (2), 314−330.

(13) de Siqueira, E. C.; de França, J. A. A.; de Souza, R. F. M.; da Silva Leoterio, D. M.; Cordeiro, J. N.; Doboszewski, B. Recent advances in the development of the physically crosslinked hydrogels and their biomedical applications. *Res., Soc. Dev.* **2023**, *12* (8), No. e18212843073.

(14) Charaya, H.; Li, X.; Jen, N.; Chung, H. J. Specific Ion Effects in Polyampholyte Hydrogels Dialyzed in Aqueous Electrolytic Solutions. *Langmuir* **2019**, *35* (5), 1526−1533.

(15) Ren, Y.; Wang, Q.; Xu, W.; Yang, M.; Guo, W.; He, S.; Liu, W. Alginate-based hydrogels mediated biomedical applications: A review. *Int. J. Biol. Macromol.* **2024**, *279* (Pt 1), No. 135019.

(16) Kopeček, J.; Yang, J. Peptide-directed self-assembly of hydrogels. *Acta Biomater.* **2009**, *5* (3), 805−816.

(17) Bustamante-Torres, M.; Romero-Fierro, D.; Arcentales-Vera, B.; Palomino, K.; Magana, H.; Bucio, E. Hydrogels Classification According to the Physical or Chemical Interactions and as Stimuli-Sensitive Materials. *Gels* **2021**, *7* (4), No. 182.

(18) Xu, R.; Ooi, H. S.; Bian, L.; Ouyang, L.; Sun, W. Dynamic hydrogels for biofabrication: A review. *Biomaterials* **2025**, *320*, No. 123266.

(19) Han, Y.; Cao, Y.; Lei, H. Dynamic Covalent Hydrogels: Strong yet Dynamic. *Gels* **2022**, *8* (9), No. 577.

(20) Zhang, K.; Feng, Q.; Fang, Z.; Gu, L.; Bian, L. Structurally Dynamic Hydrogels for Biomedical Applications: Pursuing a Fine Balance between Macroscopic Stability and Microscopic Dynamics. *Chem. Rev.* **2021**, *121* (18), 11149−11193.

(21) Rizwan, M.; Baker, A. E. G.; Shoichet, M. S. Designing Hydrogels for 3D Cell Culture Using Dynamic Covalent Crosslinking. *Adv. Healthcare Mater.* **2021**, *10* (12), No. e2100234.

(22) Muir, V. G.; Burdick, J. A. Chemically Modified Biopolymers for the Formation of Biomedical Hydrogels. *Chem. Rev.* **2021**, *121* (18), 10908−10949.

(23) Roppolo, I.; Caprioli, M.; Pirri, C. F.; Magdassi, S. 3D Printing of Self-Healing Materials. *Adv. Mater.* **2024**, *36* (9), No. e2305537.

(24) Ollier, R. C.; Webber, M. J. Mechanoresponsive Hydrogels Emerging from Dynamic and Non-Covalent Interactions. *Adv. Mater.* **2025**, *37* (40), No. e2507397.

(25) Wang, H.; Heilshorn, S. C. Adaptable hydrogel networks with reversible linkages for tissue engineering. *Adv. Mater.* **2015**, *27* (25), 3717−3736.

(26) Morgan, F. L. C.; Fernandez-Perez, J.; Moroni, L.; Baker, M. B. Tuning Hydrogels by Mixing Dynamic Cross-Linkers: Enabling Cell-Instructive Hydrogels and Advanced Bioinks. *Adv. Healthcare Mater.* **2022**, *11* (1), No. e2101576.

(27) Franse, M. W. C. P.; Nijenhuis, K. T. Crosslinking index, molecular weight distribution and rubber equilibrium shear modulus during polyfunctional crosslinking of existing polymer, 6 - Primary polymer with a Schulz-Zimm distribution of molecular weights. *Macromol. Theory Simul.* **2002**, *11* (3), 342−351.

(28) Hull, S. M.; Lou, J.; Lindsay, C. D.; Navarro, R. S.; Cai, B.; Brunel, L. G.; Westerfield, A. D.; Xia, Y.; Heilshorn, S. C. 3D bioprinting of dynamic hydrogel bioinks enabled by small molecule modulators. *Sci. Adv.* **2023**, *9* (13), No. eade7880.

(29) Zhang, V.; Accardo, J. V.; Kevlishvili, I.; Woods, E. F.; Chapman, S. J.; Eckdahl, C. T.; Stern, C. L.; Kulik, H. J.; Kalow, J. A. Tailoring Dynamic Hydrogels by Controlling Associative Exchange Rates. *Chem* **2023**, *9* (8), 2298−3317.

(30) Hafeez, S.; Ooi, H. W.; Morgan, F. L. C.; Mota, C.; Dettin, M.; Van Blitterswijk, C.; Moroni, L.; Baker, M. B. Viscoelastic Oxidized Alginates with Reversible Imine Type Crosslinks: Self-Healing, Injectable, and Bioprintable Hydrogels. *Gels* **2018**, *4* (4), No. 85.
(31) Anseth, K. S.; Klok, H. A. Click Chemistry in Biomaterials, Nanomedicine, and Drug Delivery. *Biomacromolecules* **2016**, *17* (1), 1−3.
(32) Terriac, L.; Helesbeux, J. J.; Maugars, Y.; Guicheux, J.; Tibbitt, M. W.; Delplace, V. Boronate Ester Hydrogels for Biomedical Applications: Challenges and Opportunities. *Chem. Mater.* **2024**, *36* (14), 6674−6695.
(33) Springsteen, G.; Wang, B. A detailed examination of boronic acid−diol complexation. *Tetrahedron* **2002**, *58* (26), 5291−5300.
(34) Bosch, L. I.; Fyles, T. M.; James, T. D. Binary and ternary phenylboronic acid complexes with saccharides and Lewis bases. *Tetrahedron* **2004**, *60* (49), 11175−11190.
(35) Kang, B.; Kalow, J. A. Internal and External Catalysis in Boronic Ester Networks. *ACS Macro Lett.* **2022**, *11* (3), 394−401.
(36) Chen, M.; Ren, X.; Dong, L.; Li, X.; Cheng, H. Preparation of dynamic covalently crosslinking keratin hydrogels based on thiol/disulfide bonds exchange strategy. *Int. J. Biol. Macromol.* **2021**, *182*, 1259−1267.
(37) Zhang, Y.; Qi, Y.; Ulrich, S.; Barboiu, M.; Ramstrom, O. Dynamic Covalent Polymers for Biomedical Applications. *Mater. Chem. Front* **2020**, *4* (2), 489−506.
(38) LeSavage, B. L.; Suhar, N. A.; Madl, C. M.; Heilshorn, S. C. Production of Elastin-like Protein Hydrogels for Encapsulation and Immunostaining of Cells in 3D. *J. Visualized Exp* **2018**, No. 135, No. 57739.
(39) Wade, R. J.; Burdick, J. A. Engineering ECM signals into biomaterials. *Mater. Today* **2012**, *15* (10), 454−459.
(40) Hunt, D. R.; Klett, K. C.; Mascharak, S.; Wang, H.; Gong, D.; Lou, J.; Li, X.; Cai, P. C.; Suhar, R. A.; Co, J. Y.; LeSavage, B. L.; Foster, A. A.; Guan, Y.; Amieva, M. R.; Peltz, G.; Xia, Y.; Kuo, C. J.; Heilshorn, S. C. Engineered Matrices Enable the Culture of Human Patient-Derived Intestinal Organoids. *Adv. Sci.* **2021**, *8* (10), No. 2004705.
(41) de Paiva Narciso, N.; Navarro, R. S.; Gilchrist, A. E.; Trigo, M. L. M.; Aviles Rodriguez, G.; Heilshorn, S. C. Design Parameters for Injectable Biopolymeric Hydrogels with Dynamic Covalent Chemistry Crosslinks. *Adv. Healthcare Mater.* **2023**, *12* (27), No. e2301265.
(42) Roth, J. G.; Huang, M. S.; Navarro, R. S.; Akram, J. T.; LeSavage, B. L.; Heilshorn, S. C. Tunable hydrogel viscoelasticity modulates human neural maturation. *Sci. Adv.* **2023**, *9* (42), No. eadh8313.
(43) Suhar, R. A.; Doulames, V. M.; Liu, Y.; Hefferon, M. E.; Figueroa, O., 3rd; Buabbas, H.; Heilshorn, S. C. Hyaluronan and elastin-like protein (HELP) gels significantly improve microsphere retention in the myocardium. *Biomater. Sci.* **2022**, *10* (10), 2590−2608.
(44) LeSavage, B. L.; Zhang, D.; Huerta-López, C.; Gilchrist, A. E.; Krajina, B. A.; Karlsson, K.; Smith, A. R.; Karagyozova, K.; Klett, K. C.; Huang, M. S.; Long, C.; Kaber, G.; Madl, C. M.; Bollyky, P. L.; Curtis, C.; Kuo, C. J.; Heilshorn, S. C. Engineered matrices reveal stiffness-mediated chemoresistance in patient-derived pancreatic cancer organoids. *Nat. Mater.* **2024**, *23* (8), 1138−1149.
(45) Madl, C. M.; Wang, Y. X.; Holbrook, C. A.; Su, S.; Shi, X.; Byfield, F. J.; Wicki, G.; Flaig, I. A.; Blau, H. M. Hydrogel biomaterials that stiffen and soften on demand reveal that skeletal muscle stem cells harbor a mechanical memory. *Proc. Natl. Acad. Sci. U.S.A.* **2024**, *121* (35), No. e2406787121.
(46) Discher, D. E.; Janmey, P.; Wang, Y. L. Tissue cells feel and respond to the stiffness of their substrate. *Science* **2005**, *310* (5751), 1139−1143.
(47) Courbot, O.; Elosegui-Artola, A. The role of extracellular matrix viscoelasticity in development and disease. *npj Biol. Phys. Mech.* **2025**, *2* (1), No. 10.
(48) Chaudhuri, O.; Gu, L.; Darnell, M.; Klumpers, D.; Bencherif, S. A.; Weaver, J. C.; Huebsch, N.; Mooney, D. J. Substrate stress relaxation regulates cell spreading. *Nat. Commun.* **2015**, *6*, No. 6364.
(49) Wang, H.; Zhu, D.; Paul, A.; Cai, L.; Enejder, A.; Yang, F.; Heilshorn, S. C. Covalently adaptable elastin-like protein - hyaluronic acid (ELP - HA) hybrid hydrogels with secondary thermoresponsive crosslinking for injectable stem cell delivery. *Adv. Funct. Mater.* **2017**, *27* (28), No. 1605609.
(50) Gilchrist, A. E.; Liu, Y.; Klett, K.; Liu, Y.-C.; Ceva, S.; Heilshorn, S. C. Transient Competitors to Modulate Dynamic Covalent Cross-Linking of Recombinant Hydrogels. *Chem. Mater.* **2023**, *35* (21), 8969−8983.
(51) Brooke, D.; Movahed, N.; Bothner, B. Universal buffers for use in biochemistry and biophysical experiments. *AIMS Biophys.* **2015**, *2* (3), 336−342.
(52) Dirksen, A.; Dirksen, S.; Hackeng, T. M.; Dawson, P. E. Nucleophilic Catalysis of Hydrazone Formation and Transimination: Implications for Dynamic Covalent Chemistry. *J. Am. Chem. Soc.* **2006**, *128* (49), 15602−15603.
(53) Kokubo, T. Bioactive glass ceramics: properties and applications. *Biomaterials* **1991**, *12* (2), 155−163.
(54) Kokubo, T.; Takadama, H. How useful is SBF in predicting in vivo bone bioactivity? *Biomaterials* **2006**, *27* (15), 2907−2915.
(55) Eagle, H. The specific amino acid requirements of a human carcinoma cell (Stain HeLa) in tissue culture. *J. Exp. Med.* **1955**, *102* (1), 37−48.
(56) Dulbecco, R.; Freeman, G. Plaque production by the polyoma virus. *Virology* **1959**, *8* (3), 396−397.
(57) Bayrak, Ö.; Asl, H. G.; Ak, A. Comparison of SBF and DMEM in terms of electrochemical properties of common metallic biomaterials. *Mater. Corros.* **2020**, *71* (2), 209−221.
(58) Lee, J. T.; Leng, Y.; Chow, K. L.; Ren, F.; Ge, X.; Wang, K.; Lu, X. Cell culture medium as an alternative to conventional simulated body fluid. *Acta Biomater.* **2011**, *7* (6), 2615−2622.
(59) Hui, E.; Gimeno, K. I.; Guan, G.; Caliari, S. R. Spatiotemporal Control of Viscoelasticity in Phototunable Hyaluronic Acid Hydrogels. *Biomacromolecules* **2019**, *20* (11), 4126−4134.
(60) Tang, S. C.; Richardson, B. M.; Anseth, K. S. Dynamic covalent hydrogels as biomaterials to mimic the viscoelasticity of soft tissues. *Prog. Mater. Sci.* **2021**, *120*, No. 100738.
(61) Walter, D. I.; Moore, J. W.; Sharma, A.; Stowers, R. S. Extracellular Matrix Viscoelasticity Regulates Mammary Branching Morphogenesis. *Adv. Sci.* **2026**, *13*, No. e12873.
(62) Huang, M. S.; LeSavage, B. L.; Ghorbani, S.; Gilchrist, A. E.; Roth, J. G.; Huerta-Lopez, C.; Mozipo, E. A.; Navarro, R. S.; Heilshorn, S. C. Viscoelastic N-cadherin-like interactions maintain neural progenitor cell stemness within 3D matrices. *Nat. Commun.* **2025**, *16* (1), No. 5213.
(63) Liu, Z.; Ling, S. D.; Liang, K.; Chen, Y.; Niu, Y.; Sun, L.; Li, J.; Du, Y. Viscoelasticity of ECM and cells-origin, measurement and correlation. *Mechanobiol. Med.* **2024**, *2* (4), No. 100082.
(64) Urry, D. W. Free energy transduction in polypeptides and proteins based on inverse temperature transitions. *Prog. Biophys. Mol. Biol.* **1992**, *57* (1), 23−57.
(65) Urry, D. W.; Trapane, T. L.; Prasad, K. U. Phase-structure transitions of the elastin polypentapeptide-water system within the framework of composition-temperature studies. *Biopolymers* **1985**, *24* (12), 2345−2356.
(66) Lee, J.; Macosko, C. W.; Urry, D. W. Phase transition and elasticity of protein-based hydrogels. *J. Biomater. Sci. Polym. Ed.* **2001**, *12* (2), 229−242.
(67) Cho, Y.; Zhang, Y.; Christensen, T.; Sagle, L. B.; Chilkoti, A.; Cremer, P. S. Effects of Hofmeister anions on the phase transition temperature of elastin-like polypeptides. *J. Phys. Chem. B* **2008**, *112* (44), 13765−13771.
(68) Urry, D. W.; Luan, C. H.; Parker, T. M.; Gowda, D. C.; Prasad, K. U.; Reid, M. C.; Safavy, A. Temperature of Polypeptide Inverse Temperature Transition Depends on Mean Residue Hydrophobicity. *J. Am. Chem. Soc.* **1991**, *113* (11), 4346−4348.

(69) Reguera, J.; Urry, D. W.; Parker, T. M.; McPherson, D. T.; Rodríguez-Cabello, J. C. Effect of NaCl on the exothermic and endothermic components of the inverse temperature transition of a model elastin-like polymer. *Biomacromolecules* **2007**, *8* (2), 354−358.
(70) Navarro, R. S.; Huang, M. S.; Roth, J. G.; Hubka, K. M.; Long, C. M.; Enejder, A.; Heilshorn, S. C. Tuning Polymer Hydrophilicity to Regulate Gel Mechanics and Encapsulated Cell Morphology. *Adv. Healthcare Mater.* **2022**, *11* (13), No. e2200011.
(71) Meco, E.; Lampe, K. J. Impact of Elastin-like Protein Temperature Transition on PEG-ELP Hybrid Hydrogel Properties. *Biomacromolecules* **2019**, *20* (5), 1914−1925.
(72) Yuan, Y. C.; Raheja, K.; Milbrandt, N. B.; Beilharz, S.; Tene, S.; Oshabaheebwa, S.; Gurkan, U. A.; Samia, A. C. S.; Karayilan, M. Thermoresponsive polymers with LCST transition: synthesis, characterization, and their impact on biomedical frontiers. *RSC Appl. Polym.* **2023**, *1* (2), 158−189.
(73) Pasparakis, G.; Tsitsilianis, C. LCST polymers: Thermoresponsive nanostructured assemblies towards bioapplications. *Polymer* **2020**, *211*, No. 123146.
(74) Tanaka, N.; Suyama, K.; Tomohara, K.; Nose, T. Exploring LCST- and UCST-like Behavior of Branched Molecules Bearing Repeat Units of Elastin-like Peptides as Side Components. *Biomacromolecules* **2024**, *25* (11), 7156−7166.
(75) Kunz, W.; Lo Nostro, P.; Ninham, B. W. The present state of affairs with Hofmeister effects. *Curr. Opin. Colloid Interface Sci.* **2004**, *9* (1−2), 1−18.
(76) Zhang, Y. J.; Cremer, P. S. Interactions between macromolecules and ions: the Hofmeister series. *Curr. Opin. Chem. Biol.* **2006**, *10* (6), 658−663.
(77) Taha, M.; Lee, M. J. Interactions of TRIS [tris-(hydroxymethyl)aminomethane] and related buffers with peptide backbone: Thermodynamic characterization. *Phys. Chem. Chem. Phys.* **2010**, *12* (39), 12840−12850.
(78) Mirzaei, S.; Mobedi, H.; Gourabi, H.; Sanati, M. H.; Khezli, S.; Ighaeie, M.; Omidian, H. Enhancement of The Stability of Human Growth Hormone by Using Tris(hydroxymethyl)aminomethane: Molecular Docking and Experimental Analysis. *Cell J.* **2021**, *22* (4), 406−414.
(79) Mao, T.; Xu, X. F.; Winkler, P. M.; Siri, C.; Poliukhina, E.; Silva, P. J.; Xu, N.; Hu, Y.; Al Zahabi, K.; La Polla, R.; Luo, Z.; Ong, Q.; Alexander-Katz, A.; Stellacci, F. Stabilizing effect of amino acids on protein and colloidal dispersions. *Nature* **2025**, *645* (8082), 915−921.
(80) Oshima, H.; Kinoshita, M. Effects of sugars on the thermal stability of a protein. *J. Chem. Phys.* **2013**, *138* (24), No. 245101.
(81) Stasiulewicz, M.; Panuszko, A.; Bruzdziak, P.; Stangret, J. Mechanism of Osmolyte Stabilization-Destabilization of Proteins: Experimental Evidence. *J. Phys. Chem. B* **2022**, *126* (16), 2990−2999.
(82) Sorichetti, V.; Ninarello, A.; Ruiz-Franco, J. M.; Hugouvieux, V.; Kob, W.; Zaccarelli, E.; Rovigatti, L. Effect of Chain Polydispersity on the Elasticity of Disordered Polymer Networks. *Macromolecules* **2021**, *54* (8), 3769−3779.
(83) Onogi, S.; Kimura, S.; Kato, T.; Masuda, T.; Miyanaga, N. Effects of Molecular Weight and Concentration on Flow Properties of Concentrated Polymer Solutions. *J. Polym. Sci. Polym. Sym.* **1966**, *15* (15), 381−406.
(84) Musilová, L.; Mracek, A.; Kaspárková, V.; Minaríik, A.; Valente, A. J. M.; Azevedo, E. F. G.; Veríssimo, L. M. P.; Rodrigo, M. M.; Esteso, M. A.; Ribeiro, A. C. F. Effect of Hofmeister Ions on Transport Properties of Aqueous Solutions of Sodium Hyaluronate. *Int. J. Mol. Sci.* **2021**, *22* (4), No. 1932.
(85) Mráček, A.; Varhaníková, J.; Lehocky, M.; Grundelová, L.; Pokopcová, A.; Velebny, V. The influence of Hofmeister series ions on hyaluronan swelling and viscosity. *Molecules* **2008**, *13* (5), 1025−1034.
(86) Horkay, F.; Basser, P. J.; Londono, D. J.; Hecht, A. M.; Geissler, E. Ions in hyaluronic acid solutions. *J. Chem. Phys.* **2009**, *131* (18), No. 184902.
(87) Giubertoni, G.; de Alba Ortíz, A. P.; Bano, F.; Zhang, X.; Linhardt, R. J.; Green, D. E.; DeAngelis, P. L.; Koenderink, G. H.; Richter, R. P.; Ensing, B.; Bakker, H. J. Strong Reduction of the Chain Rigidity of Hyaluronan by Selective Binding of Ca(2+) Ions. *Macromolecules* **2021**, *54* (3), 1137−1146.
(88) McKinnon, D. D.; Domaille, D. W.; Cha, J. N.; Anseth, K. S. Bis-Aliphatic Hydrazone-Linked Hydrogels Form Most Rapidly at Physiological pH: Identifying the Origin of Hydrogel Properties with Small Molecule Kinetic Studies. *Chem. Mater.* **2014**, *26* (7), 2382−2387.
(89) Jencks, W. P. Studies on the Mechanism of Oxime and Semicarbazone Formation1. *J. Am. Chem. Soc.* **1959**, *81* (2), 475−481.
(90) Nauman, D. A.; Bertozzi, C. R. Kinetic parameters for small-molecule drug delivery by covalent cell surface targeting. *Biochim. Biophys. Acta, Gen. Subj.* **2001**, *1568* (2), 147−154.
(91) Zeng, Y.; Ramya, T. N.; Dirksen, A.; Dawson, P. E.; Paulson, J. C. High-efficiency labeling of sialylated glycoproteins on living cells. *Nat. Methods* **2009**, *6* (3), 207−209.
(92) Kölmel, D. K.; Kool, E. T. Oximes and Hydrazones in Bioconjugation: Mechanism and Catalysis. *Chem. Rev.* **2017**, *117* (15), 10358−10376.
(93) Larsen, D.; Pittelkow, M.; Karmakar, S.; Kool, E. T. New Organocatalyst Scaffolds with High Activity in Promoting Hydrazone and Oxime Formation at Neutral pH. *Org. Lett.* **2015**, *17* (2), 274−277.
(94) Rubinstein, M.; Semenov, A. N. Thermoreversible Gelation in Solutions of Associating Polymers. 2. Linear Dynamics. *Macromolecules* **1998**, *31* (4), 1386−1397.
(95) Leibler, L.; Rubinstein, M.; Colby, R. H. Dynamics of reversible networks. *Macromolecules* **1991**, *24* (16), 4701−4707.
(96) Lou, J.; Xia, Y. Using Competitor Molecules to Reversibly Modulate the Mechanical Properties of Viscoelastic Hydrogels. *ACS Macro Lett.* **2022**, *11* (11), 1312−1316.
(97) Cai, P. C.; Su, B.; Zou, L.; Webber, M. J.; Heilshorn, S. C.; Spakowitz, A. J. Rheological Characterization and Theoretical Modeling Establish Molecular Design Rules for Tailored Dynamically Associating Polymers. *ACS Cent Sci.* **2022**, *8* (9), 1318−1327.
(98) Marco-Dufort, B.; Iten, R.; Tibbitt, M. W. Correction to "Linking Molecular Behavior to Macroscopic Properties in Ideal Dynamic Covalent Networks". *J. Am. Chem. Soc.* **2020**, *142* (43), 18730−18731.
(99) Parada, G. A.; Zhao, X. Ideal reversible polymer networks. *Soft Matter* **2018**, *14* (25), 5186−5196.
(100) Appel, E. A.; Biedermann, F.; Rauwald, U.; Jones, S. T.; Zayed, J. M.; Scherman, O. A. Supramolecular Cross-Linked Networks via Host−Guest Complexation with Cucurbit[8]uril. *J. Am. Chem. Soc.* **2010**, *132* (40), 14251−14260.
(101) Crowell, A. D.; Kang, J.; Conrad, D. L.; FitzSimons, T. M.; Anslyn, E. V.; Milliron, D. J.; Rosales, A. M. Leveraging bond dissociation kinetics to tune shear-thickening behavior in dynamic covalent tetra-PEG hydrogels. *Sci. Adv.* **2026**, *12* (10), No. eadz9563.
(102) Milisav, A. M.; Strasser, V.; Marfoglia, A.; Bojanic, K.; Erceg, I.; Christiansen, S.; Ivanic, M.; Fiket, Z.; Cazalbou, S.; Dutour Sikiric, M. Calcium Phosphate Mineralization of Bulk Alginate Hydrogels Composites With Metal and Metal Oxide Nanoparticles. *Macromol. Biosci.* **2026**, *26* (1), No. e00468.
(103) Xu, L.; Kang, H.; Wei, W.; Goto, T.; Wu, X.; Dai, H. Freezing, Salting-Out and Mineralization — A Simple, Universal and Modular Strategy for Constructing Mineralized Hydrogels. *Adv. Funct. Mater.* **2024**, *34* (41), No. 2406367.
(104) Wen, B.; Dai, Y.; Han, X.; Huo, F.; Xie, L.; Yu, M.; Wang, Y.; An, N.; Li, Z.; Guo, W. Biomineralization-inspired mineralized hydrogel promotes the repair and regeneration of dentin/bone hard tissue. *npj Regener. Med.* **2023**, *8* (1), No. 11.
(105) Wang, X.; Zhang, H. J.; Yang, Y.; Chen, Y.; Zhu, X.; You, X. Biopolymer-based self-healing hydrogels: A short review. *Giant* **2023**, *16*, No. 100188.
(106) Jaeschke, M. W.; Borelli, A. N.; Skillin, N. P.; White, T. J.; Anseth, K. S. Engineering a Hydrazone and Triazole Crosslinked

Hydrogel for Extrusion-Based Printing and Cell Delivery. *Adv. Healthcare Mater.* **2024**, *13* (20), No. e2400062.
(107) Ramimoghadam, D.; Eyckens, D. J.; Evans, R. A.; Moad, G.; Holmes, S.; Simons, R. Towards Sustainable Materials: A Review of Acylhydrazone Chemistry for Reversible Polymers. *Chemistry* **2024**, *30* (49), No. e202401728.
(108) Feng, J.; Ponomareva, P.; Liu, K.; Nie, C.; Chen, R.; Haag, R. Dual-Dynamic Covalently Cross-Linked Polyglycerol Hydrogels for Tumor Spheroid Culture. *Biomacromolecules* **2025**, *26* (6), 3331−3343.
(109) Kloxin, A. M.; Kloxin, C. J.; Bowman, C. N.; Anseth, K. S. Mechanical Properties of Cellularly Responsive Hydrogels and Their Experimental Determination. *Adv. Mater.* **2010**, *22* (31), 3484−3494.
(110) Anseth, K. S.; Bowman, C. N.; Brannon-Peppas, L. Mechanical properties of hydrogels and their experimental determination. *Biomaterials* **1996**, *17* (17), 1647−1657.
(111) Schwab, A.; Levato, R.; D'Este, M.; Piluso, S.; Eglin, D.; Malda, J. Printability and Shape Fidelity of Bioinks in 3D Bioprinting. *Chem. Rev.* **2020**, *120* (19), 11028−11055.

https://doi.org/10.1021/acs.biomac.5c02684
Biomacromolecules 2026, 27, 3222−3236